Millisecond Optical Phase Modulation using Multi-pass Configurations with Liquid Crystal Devices

Yihan Jin[1], Steve J. Elston[1, †], Julian A. J. Fells[1], Martin J. Booth[1], Chris Welch[2], Georg H. Mehl[2] and Stephen M. Morris[1,*]

[1]*Department of Engineering Science, University of Oxford, Parks Road, Oxford, OX1 3PJ, United Kingdom*

[2]*Department of Chemistry, University of Hull, Hull, HU6 7RX, United Kingdom*

[†]steve.elston@eng.ox.ac.uk
[*]stephen.morris@eng.ox.ac.uk

Abstract

We present two configurations for analogue 0 to 2π optical phase modulation using liquid crystals (LC), each of which achieve switching times that are 1 ms or less. One configuration is based on the switching behavior of a so-called nematic pi-cell, and the other is based on the flexoelectro-optic effect in chiral nematic LCs when operated in the uniform lying helix geometry. Both configurations exploit a multi-pass optical arrangement in order to enhance the available optical phase range whilst maintaining a fast switching speed. Moreover, these devices can be operated at or close to room temperature. Experimental data is found to be in good agreement with results predicted from theory for these multi-pass phase modulation configurations.

I. INTRODUCTION

Optical phase modulation is important in many aspects of optical and opto-electronic technology [1]. Phase modulation can be obtained either by changing the refractive index (or effective refractive index) of a material through which light is propagating, or by physically changing the optical path-length for the light. For applications requiring a spatially structured phase modulation of a propagating optical wave-front, a liquid crystal (LC) spatial light modulator (SLM) is often desirable and has been employed in applications such as micromanipulation and beam-shaping [2-7]. Commercial SLM technology based upon LCs broadly breaks down into two categories: those that provide a digital, binary, or quantized phase modulation with a very limited number of states (e.g. 0 and π phase states are commonly chosen) and those that provide analogue (or at least, multi-level) phase modulation (e.g. a phase range of 0 to 2π is commonly used). As an example, binary SLM technology [8-10] is often based on the bi-stable switching of ferroelectric LCs and can achieve switching times that are substantially less than 1 ms. A high-speed technology based on anti-ferroelectric LCs has recently been demonstrated, but this uses rather thick layers of LC, thus limiting the potential pixel pitch [11]. Analog SLM technology, on the other hand, typically involves switching a layer of nematic LC, but the switching times are generally much longer, being many milliseconds [12, 13], although with careful material and device optimisation 2 ms response times have been obtained in the laboratory [14].

Improving the switching speed, whilst maintaining access to a full range of phase states (from 0 to 2π) enables SLM technology to be used in a wider range of systems, such as in faster optical laser beam tracking/steering [15], and in higher-speed optical aberration correction in imaging systems [16]. There has been much work in this area, with a number of proposals and demonstrations of configurations which can enhance the switching speed (reduce the response

time) in a useful way. For example, two-photon laser writing techniques have been employed to engineer advanced structures inside of LC devices in order to optimise switching times [17-19], and there has been work on incorporating polymer networks into LC layers in order to obtain sub-millisecond switching times [20].

An alternative approach has been demonstrated using the flexoelectro-optic effect in chiral nematic LCs [21]. This electro-optic effect, which can be observed when an electric field is applied perpendicular to the helical axis of the chiral nematic LC, can exhibit fast electro-optic properties because the characteristic length scale is the helical pitch (which can be of the order of 100s nm) rather than the device thickness. While the electro-optic effect offers sub-millisecond switching times, the optical response is generally quite small for most LC compounds and mixtures, with switching angles of just a few degrees. Bimesogenic LCs, however, can show much larger switching angles, allowing useful electro-optic effects to be exploited [22]. Using a configuration based upon the flexoelectro-optic effect in combination with wave-plates and a reflecting element, we have shown in previous work that it is possible to achieve sub-millisecond 0 to 2π optical phase modulation [23].

A drawback with the approach demonstrated in Ref. 23 is that the devices had to be operated at somewhat elevated temperatures (in excess of 100°C), which is impractical for most technological applications. Unfortunately, room-temperature materials showing a large and high-speed flexoelectro-optic effect are not yet commonly available. An LC which shows substantial switching angles at room temperature has recently been demonstrated, but it requires large electric fields (equivalent to 100V across a 5 μm-thick device to achieve a switching angle of 40°) [22]. Therefore, there is still considerable value in identifying new modes and configurations that can lead to fast switching and full 2π phase modulation. The

focus of this work, therefore, is to report on two alternative approaches that potentially address the shortcomings that are present in existing technologies. Namely, full 2π phase modulation operating at switching frequencies much greater than 100 Hz at room temperature.

II. ALTERNATIVE CONFIGURATIONS

In the first configuration, a nematic electro-optic mode is used in a high-speed regime. For nematic LCs the "switch-off" speed is typically the limiting factor in engineering a high-speed optical response. This is because the "switch-on" is driven by an applied voltage and the resulting switching speed is primarily controlled by the corresponding electric field and the viscosity of the LC. Therefore, by ensuring that the field is sufficiently large, high-speed switching can be obtained. However, the "switch-off" speed [24] is primarily controlled by the elasticity and viscosity of the LC, and therefore this is harder to control, other than through material parameter optimization [25]. Alternatively, the switching speed can be improved through the use of polymer stabilization [26] or by making the device thinner. Polymer stabilization, while it can be effective, often leads to larger driving voltages and increased light scattering, both of which are unwanted side effects. Making the device thinner is a possible solution as the thickness of a nematic LC layer strongly influences the switching speed. In general, the characteristic "switch-off" time constant, τ, is given by $\tau \approx {\gamma d^2}/{\pi^2 K}$ [24], where γ is the rotational viscosity, K is an elastic constant, and d is the layer thickness. Therefore, a thin layer thickness (d) leads to high-speed switching.

There are, however, two problems with the approach of reducing the layer thickness: (i) thin uniform layers are more difficult to engineer, and the devices become difficult to capillary fill; (ii) thin layers show a reduced electro-optic effect, so the degree of phase

modulation available may be insufficient. Here we aim to address these two issues. Firstly, we use an LC layer with a conventional device thickness of 5 microns but exploit the switching of a thin region near the surfaces of the device. Secondly, we use a multi-pass optical arrangement to enhance the electro-optic effect at the surfaces of the device to obtain a full 0 to 2π optical phase modulation.

For the second configuration, a room temperature flexoelectro-optic device is employed that exhibits small angle deflection, but the electro-optic response is enhanced (or amplified) through a multi-pass configuration. In our previous work using the flexoelectro-optic effect we have shown that by integrating the LC layer between quarter-wave plates and a mirror it is possible to obtain full 0 to 2π optical phase modulation in a device with a switching angle of ±45° [23]. However, as noted, fast-switching materials that operate at room temperature tend to show reduced switching angles. In this study, we use a bimesogenic-doped eutectic mixture that exhibits switching angles in the range of ±15° to ±20° at room temperature and demonstrate that enhanced optical phase modulation can be obtained by using a multi-pass geometry.

III. THEORETICAL CONSIDERATIONS

A. Phase modulation with a nematic pi-cell

In a layer of nematic LC with positive dielectric anisotropy the application of an electric field across the layer causes reorientation of the director from a planar state towards a state with the director oriented perpendicular to the device surfaces. At high voltages the bulk of the layer is reoriented to the perpendicular state, and small transition regions (or boundary layers) remain near the device surfaces which are shown in **FIG. 1**.

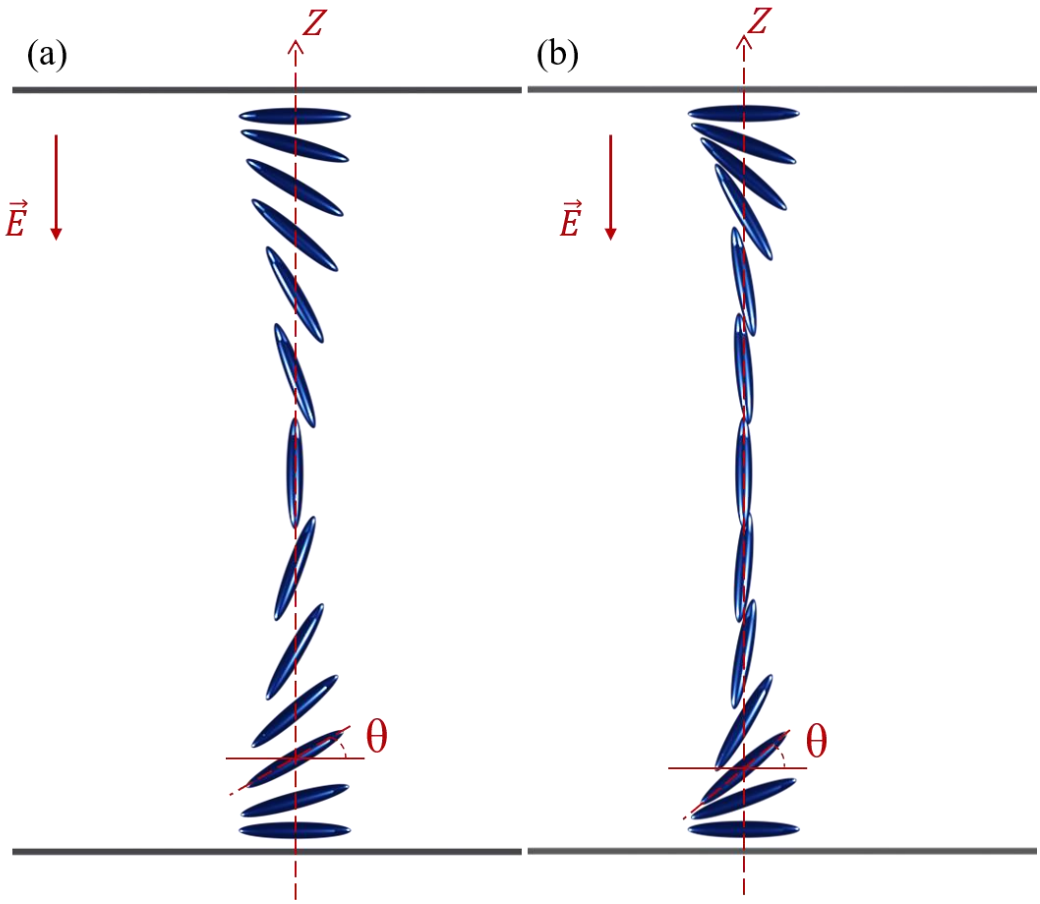

FIG. 1. The orientation of a nematic LC director when subjected to an applied electric field in a pi-cell. The orthographic side view of the pi-cell device at (a) low voltage and (b) high voltage. The direction of the electric field in both cases is parallel to the normal of the substrates.

In a conventional anti-parallel rubbed device that exhibits the well-known Fréedericksz threshold voltage, the director tilt in the boundary layers is in the same sense near the two surfaces. On the other hand, in the so-called pi-cell (parallel rubbed surfaces) [28] the tilt is in the opposite sense in the two boundary layers. In the limit of very high voltages, and if the tilt of the director out of the cell surface plane is given by the angle θ (the tilt angle θ and coordinate Z are defined as in **FIG. 1**), then these states can be written as

$$z = 0 : \theta = 0°$$
$$0 < z < d : \theta = 90°$$
$$z = d : \theta = 0°$$

for the Fréedericksz device and

$$z = 0 : \theta = 0°$$
$$0 < z < d : \theta = 90°$$
$$z = d : \theta = 180°$$

for the pi-cell device, where *z* measures the position through the LC layer.

In each case, when the electric field is removed, relaxation of the director from the switched state back towards the planar state begins from the surfaces. If we use a simple one elastic constant approximation (i.e. $K_{11} = K_{22} = K_{33} = K$) to model the LC behavior then the initial response of the boundary layers at each surface has an analytic solution in terms of the error-function (erf) of the form

$$\theta(z,t) = \theta_s + (\theta_b - \theta_s)\mathrm{erf}\left\{\frac{z\sqrt{\gamma}}{2\sqrt{K}\sqrt{t}}\right\} \quad (1)$$

where *z* is now a coordinate measured from the surface, θ_s and θ_b are the initial surface and bulk director orientations, respectively, and *K* is the LC elastic constant. This solution is valid at each surface for short timescales provided that the erf{...} term remains close to unity for $z = d/2$.

To determine the magnitude of the optical phase change (modulation) available through this boundary layer behaviour we need to determine the phase, ϕ, of the light propagating through the LC,

$$\phi = \frac{2\pi}{\lambda}\int_0^d n_{eff}(z)\mathrm{d}z \quad (2)$$

where

$$n_{eff}(z) = \sqrt{n_e^2\cos^2(\theta) + n_o^2\sin^2(\theta)} \quad (3)$$

Here λ is the wavelength of light, and n_e and n_o are the extraordinary and ordinary refractive indices of the LC, respectively. Further analytic progress is challenging because the integration of the trigonometric function of the error function is non-trivial. However, further progress can

be made if: (a) we introduce a piecewise linear approximation to the error function of the following form:

$$\mathrm{erf}(u) \approx \frac{u}{u_0} \;:\; u < u_0 \tag{4}$$

$$\mathrm{erf}(u) \approx 1 \;:\; u \geq u_0 \tag{5}$$

where u_0 is chosen such that the integral of the approximation to the error function remains correct (leading to u_0 =1.12838); and (b) we also expand $n_{eff}(z)$ for small Δn.

Assuming that $\theta_s = 0°$ and $\theta_b = 90°$, $\theta(z,t)$ can now be written as

$$\theta(z,t) \approx 90° \cdot \frac{1}{1.12838} \cdot \frac{z\sqrt{\gamma}}{2\sqrt{K}\sqrt{t}} \quad \text{for} \quad \frac{z\sqrt{\gamma}}{2\sqrt{K}\sqrt{t}} < 1.12838 \tag{6}$$

$$\theta(z,t) \approx 90° \quad \text{for} \quad \frac{z\sqrt{\gamma}}{2\sqrt{K}\sqrt{t}} \geq 1.12838 \tag{7}$$

and

$$n_{eff}(z) \approx n_o \left(1 + \frac{A}{2}\cos^2(\theta) - \frac{A^2}{8}\cos^4(\theta) + \cdots\right) \tag{8}$$

where

$$A = \frac{n_e^2 - n_o^2}{n_o^2} \tag{9}$$

Substituting these into Equation (2) allows ϕ to be determined as

$$\phi = \frac{2\pi}{\lambda}\left\{n_o d + 2n_o z_{crit}\left(\frac{A}{4} - \frac{3A^2}{64} + \cdots\right)\right\} \tag{10}$$

where

$$z_{crit} = 1.12838 \cdot \frac{2\sqrt{K}\sqrt{t}}{\sqrt{\gamma}} \tag{11}$$

In Equation (10), the first term in the curly brackets (the $n_o d$ term) represents a fixed phase term whereas the other terms represent a change in the phase. Setting the phase change to π/2 and using light of wavelength λ = 632.8 nm (He-Ne laser), together with the physical parameters for the nematic LC, E7, allows us to determine a time that represents a response for a π/2 phase modulation[1], which is then estimated to be $t \approx$ 1ms. We note that this response

[1] There is some variation in the published parameters for E7. Based on the elastic constants published in [28] we use a one-constant approximation of $K \approx$ 15pN. The rotational viscosity published in [28] is $\gamma \approx$ 0. 08Pa.s, but values published elsewhere are typically higher. Here

time is independent of the thickness of the LC device provided that its thickness is substantially greater than twice z_{crit} at this point in time, which is 0.7 μm for the above case.

The implication of these findings is that π/2 phase modulation is available on a millisecond timescale in the "switch-off" (relaxation) of nematic layers provided that they are switched on at high voltage. In the experimental section this behaviour is demonstrated using a pi-cell device. By using a multi-pass configuration, the phase modulation is then enhanced to give a full 0 to 2π range.

B. Phase modulation with flexoelectro-optic switching

In the flexoelectro-optic effect, the applied electric field leads to an in-plane rotation of the effective optic axis of the helical structure by an angle, χ (the definition is shown in **FIG. 2 (b)**), which to first order is given by [30]

$$\chi = \frac{e_1 - e_3}{K_{11} + K_{33}} \frac{E}{q} \tag{12}$$

where e_1 and e_3 are the splay and bend flexoelectric coefficients, respectively, K_{11} and K_{33} are the splay and bend elastic constants, respectively, E is the applied electric field, and $q = 2\pi/p$, where p is the pitch of the chiral nematic helix. The orientation of the chiral nematic LCs without and with an applied electric field are shown in **FIG. 2**.

we used a value of $\gamma \approx 0.15$Pa.s. We use $n_o = 1.52$, $n_e = 1.74$ from [29]. (All values quoted at room temperature.)

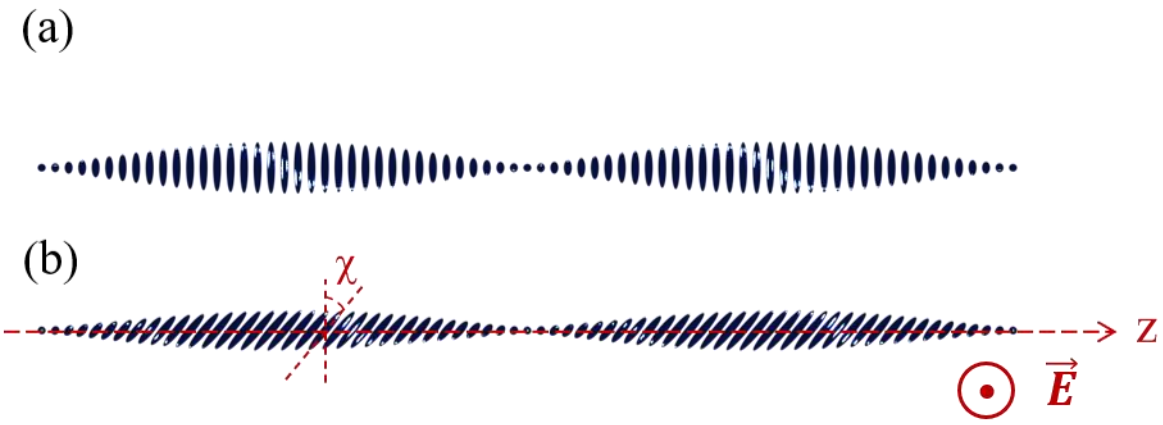

FIG. 2. Definition of the geometrical quantities (tilt angle χ and coordinate Z) for the configuration based on the flexoelectro-optic effect. Device without (a) and with (b) an applied electric field applied perpendicular to the helix axis.

If the layer of LC is placed between quarter-wave plates, there is a modulation in the phase of the transmitted light. The magnitude of this phase modulation can be determined using a Jones matrix [31] approach via

$$\boldsymbol{E}_{\text{out}} = \boldsymbol{Q}\left(-\frac{\pi}{4}\right)\boldsymbol{LC}(\chi)\boldsymbol{Q}\left(+\frac{\pi}{4}\right)\boldsymbol{E}_{\text{in}} \tag{13}$$

where $\boldsymbol{E}_{\text{in}}$ is the incoming light field, $\boldsymbol{Q}\left(\pm\frac{\pi}{4}\right)$ are quarter-wave plates at ±45°, $\boldsymbol{LC}(\chi)$ is the flexoelectro-optic LC layer switched to an angle χ, and $\boldsymbol{E}_{\text{out}}$ is the outgoing light field. Using Equation (13) it can be demonstrated that the optical phase modulation is twice the switching angle of the effective optic axis in the LC layer. So, if the switching angle is $\pm\chi_{\text{max}}$ then the phase modulation obtained is $\pm 2\chi_{\text{max}}$. Placing a reflector (mirror) behind this system of components, and using the modulator in a reflective mode doubles this further, giving a phase modulation of $\pm 4\chi_{\text{max}}$. Therefore, with a switching range of ±45° a phase range of $\pm\pi$ is available (equivalent to a full optical phase range of 0 to 2π).

This principle can be extended further to a "multi-pass" concept. The single-pass, as shown by Equation (13), leads to a phase modulation of $\pm 2\chi_{max}$. The reflection configuration used in previous work [23] is effectively a double-pass arrangement leading to twice this modulation, i.e., $\pm 4\chi_{max}$. Therefore, a three-pass arrangement would lead to $\pm 6\chi_{max}$, and a four-pass arrangement would lead to $\pm 8\chi_{max}$, and so on. In the present study we demonstrate the enhancement of the phase modulation by increasing from a single, to a double and finally a four-pass arrangement.

IV. EXPERIMENTAL RESULTS AND DISCUSSION

A. Nematic Pi-cell Phase Modulator

To begin with, we demonstrate the high-speed switching in a nematic pi-cell. The pi-cell's surfaces were treated so that they can provide a surface alignment that will create the same pretilt direction on both surfaces so that the flow results in no torque being applied to the LC director in the centre of the cell [27]. For this work the nematic eutectic mixture, E7 (Synthon Ltd), was capillary filled into a pi-cell, which consisted of glass substrates that were coated in indium tin oxide (ITO) electrodes and parallel rubbed polyimide alignment layers. The thickness of the device was nominally 5 μm. Placing such a device between crossed polarizers, with the alignment direction at 45° to the polarizer axis, the transmission tends to zero at high voltage. When the voltage is removed the transmission increases. At the point where the transmission reaches 50% the phase retardation of the device is equivalent to a quarter-wave plate, which is where the phase for light polarized along the alignment direction has changed by $\pi/2$. This is where the boundary layers have grown to a thickness of z_{crit} as outlined in Section IIIA.

The behaviour described here is shown in **FIG. 3** where the wavelength of light used was λ = 632.8 nm (He-Ne laser). The switching voltage waveform was a 5 kHz square-wave modulated to give a sequence of 50 V_{pp} (drive voltage), 0V (relax voltage), and 6 V_{pp} (hold voltage) (The waveform generator was a Tektronix AFG 3022). Firstly, the 50 V_{pp} switches the device on before the 0V then allows the boundary layers to grow from the surface. At the point where the transmission reaches 50% a holding voltage of 6 V_{pp} was applied. The sequence was then repeated. Importantly, the time to "relax" to a transmission of 50% was found to be 0.75ms. This is actually slightly less than the equivalent time for $\pi/2$ phase modulation estimated in Section IIIa, but it should be remembered that this was based on a simplified analytic approach.

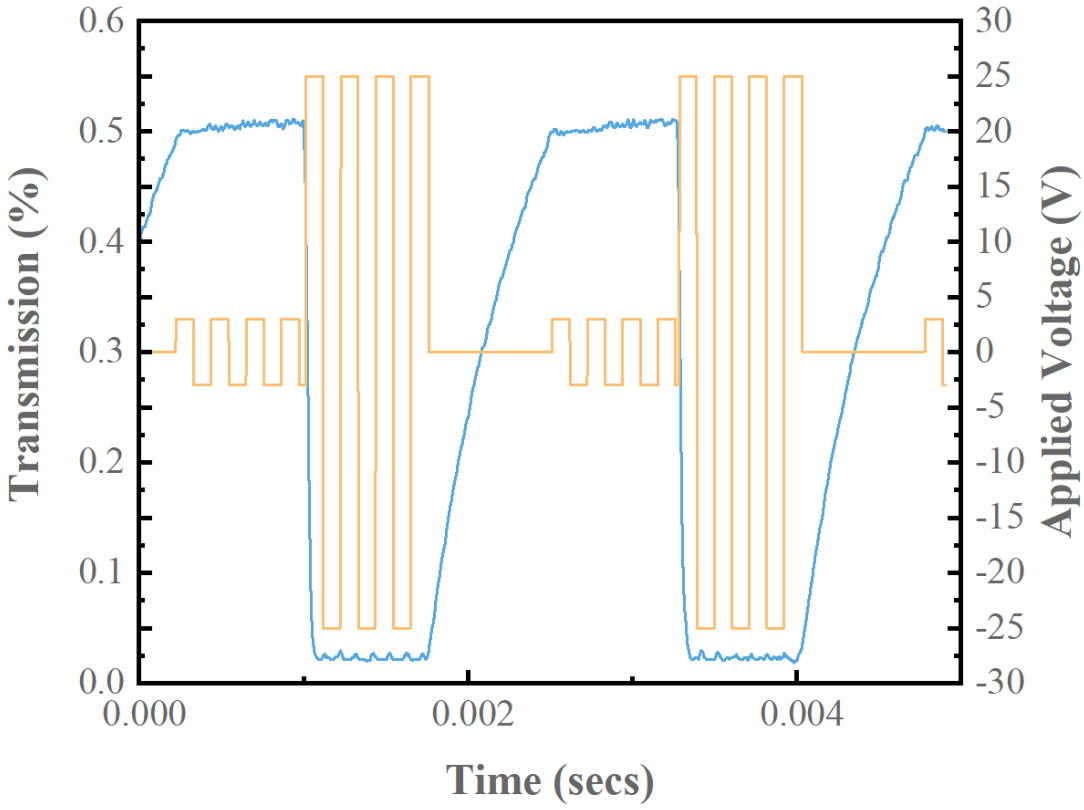

FIG. 3. Transmission as a function of time (blue solid line) for a nematic pi-cell between crossed polarizers when the device was driven by the voltage waveform sequence shown by the orange solid line and as described in the main text. Modulation of the transmission by 50% corresponds to a phase change of $\pi/2$ in the extraordinary wave.

Next, we placed the pi-cell device in a simple Mach-Zehnder interferometer [32]. The experimental arrangement was as shown in **FIG. 4(a)**. The resulting fringes were recorded using a CCD camera as the device was switched through the sequence described previously; the time of each part of the modulated 5 kHz waveform was now set to be 1 ms (i.e. 1 ms at drive voltage, 1 ms at relax voltage, 1 ms at hold voltage, repeated). The recorded fringes were then analyzed to track the phase-change of the wavefront of the light passing through the pi-cell device. To demonstrate control of the resulting phase of the transmitted light the modulation of the $50V_{pp}$, 0V, $6V_{pp}$ sequence was then adjusted, and the phase-change tracked for each case. (Note: as the modulation of the waveform is decreased the drive voltage reduces and the relaxation voltage increases, but the overall rms voltage remains sufficient to retain the pi-state in the device.) The results are shown in **FIG. 5** where the *x*-axis shows the difference between the drive voltage and the relaxation voltage (ΔV) for different modulation depths (0% to 100%). In the figure we can see that a maximum phase modulation of slightly in excess of 90° was obtained, and that this varied smoothly as the modulation was changed. This response was obtained in 1 ms. The amplitude (or intensity) modulation in this configuration is minimal because the nematic director is switching in the plane of the incident polarized light. There are small losses due to the reflections at the device surfaces, and the small amount of optical scattering in the nematic LC, but the overall arrangement is very optically efficient.

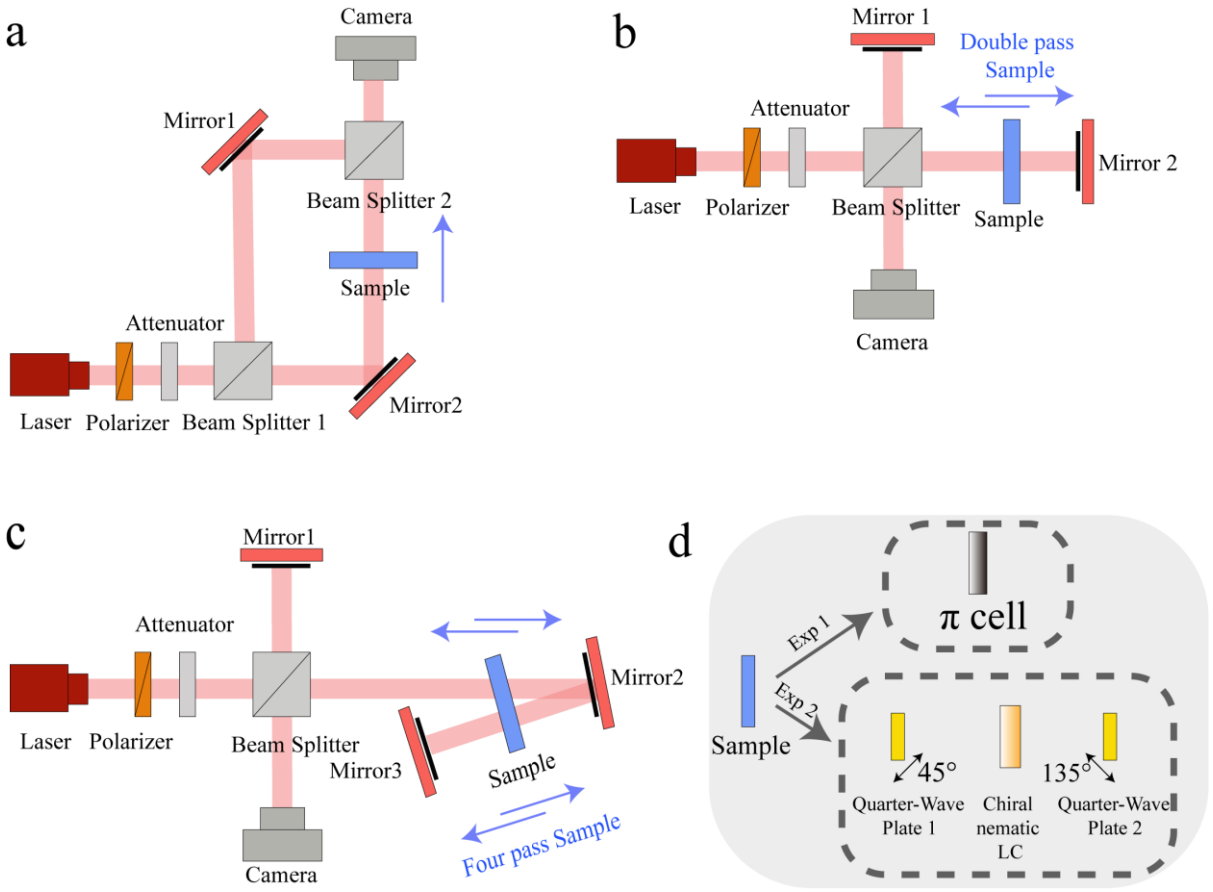

FIG. 4. Schematic diagrams of the experimental arrangements. (a) The one-pass setup (Mach-Zehnder interferometer); (b) The two-pass setup (Michelson configuration); (c) The four-pass setup ("folded" Michelson configuration); (d) The two different device geometries used: a pi-cell and a flexoelectro-optic (chiral nematic LC) device between quarter-wave plates.

FIG. 5 also shows the results from modelling the phase behaviour. A simple analytic model can be developed based on the ideas introduced in Section IIIA. In this case a piecewise linear form is again used, but now the boundary layer thickness, z_{crit}, is determined by minimising the energy for the driving and holding voltages (this leads to the dotted black line in **FIG. 5**). Alternatively, rather than using the analytic estimation outlined in Section IIIA, a model can be based on a finite-difference numerical solution to the Euler-Lagrange equations for simple nematic continuum theory. Only the splay and bend elastic constants are relevant in this model (values of K_{11} = 11.1 pN and K_{33} = 17.1 pN were used for E7 [28], this leads to the orange dashed line in **FIG. 5**). The device thickness was 5 microns, $\Delta\varepsilon$ = 14.0, and Δn = 0.22.

It can be seen that the simple analytic model is reasonable at lower modulation levels, but diverges substantially at higher modulation levels. This may be because the dynamic behaviour becomes more important in these cases. For the numerical model it can be seen that whilst the overall trend is reasonable, the model falls slightly outside of the error bars associated with the experimental data (measurement of optical phase from the interferometer). It is not entirely clear why this is so, although it may be due to the lack of inclusion of flow in our model, this being generally considered to enhance the switching speeds in pi-cells [33]. (Some allowance for this effect was included by reducing the rotational viscosity for the fit, where a value of $\gamma = 0.07$ Pa.s was used, which is very similar to the value quoted in [28]). In subsequent graphs we show only the results from the numerical modelling alongside the experimental results.

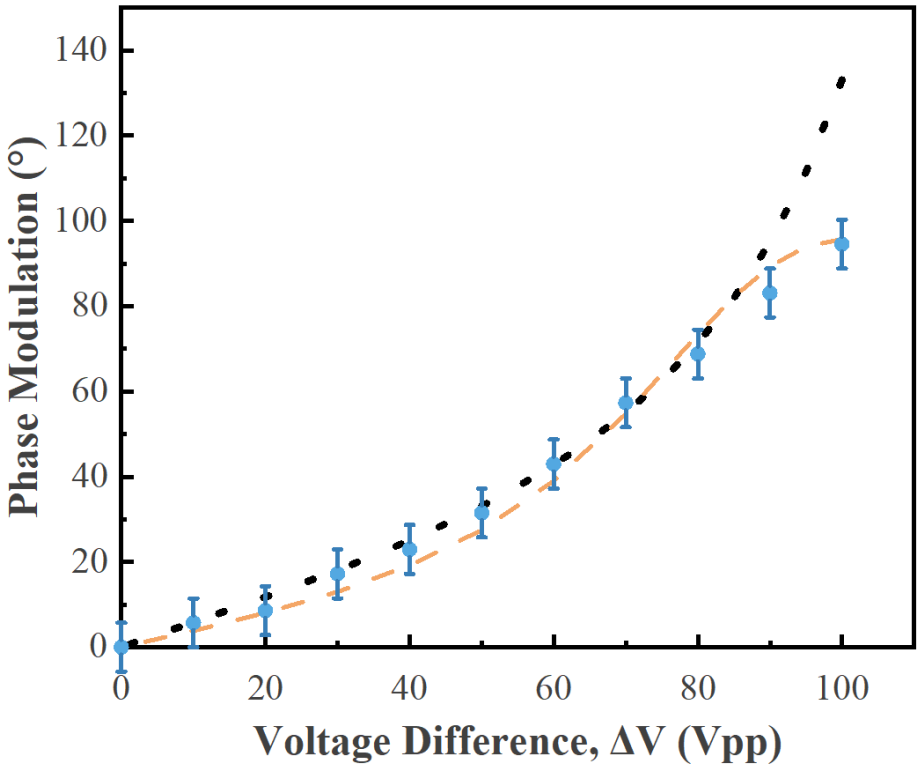

FIG. 5. Phase modulation obtained using a pi-cell, driven by the waveform sequence as described in the main text. The data points (blue circles) are from the experiments and the dashed orange line represents the results from the numerical model. The dotted black line shows the results from a simplified analytic model.

For the geometry considered here, light is only passing through the device once (i.e. it is a one-pass configuration). Next, we re-configure the interferometer into a Michelson configuration [34] and place the device in one arm to give a two-pass arrangement. The diagram of the two-pass set up is shown in **FIG. 4(b)**. The light then passes through the device twice, and an enhanced optical phase modulation effect is obtained. The results, for the same driving conditions used previously, are shown in **FIG. 6(a)**. We can see from the figure that the behaviour follows the same trend as that shown in **FIG. 5**, but that the optical phase modulation is now twice as much, reaching a maximum in excess of 180° (π).

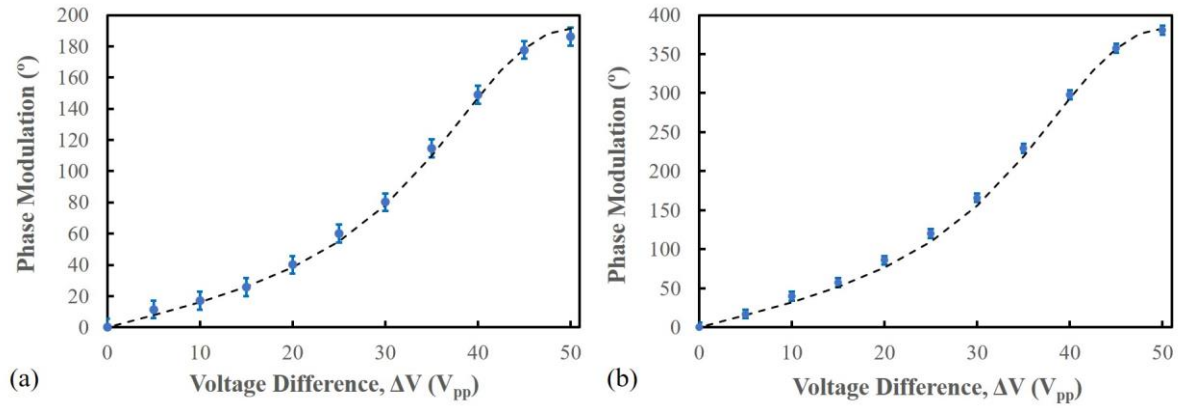

FIG. 6. Phase modulation obtained using a pi-cell. The points are the experimental data and the dashed lines are based on the results from the model. (a) Two-pass configuration; (b) Four-pass configuration.

To increase the modulation depth further, we modify the arrangement of the interferometer to pass the light through the device four times; this is done by adding an additional mirror into the signal arm of the Michelson arrangement, the diagram is shown in **FIG. 4(c)**. The result for this four-pass configuration is shown in **FIG. 6(b)**. Here we can see that an optical phase modulation in excess of 360° (2π) is obtained. Again, we see that the experimental data lie slightly off the line of the model. However, importantly, this

configuration has demonstrated a full phase modulation of the light (i.e. a phase range of greater than 0 to 2π) with a 1 ms switching time. Even faster switching times would be available using more optimised materials, such as that used in the work by Huang et al [14].

B. Phase modulation with multi-pass flexoelectro-optic switching

For the flexoelectro-optic effect we first investigate the switching behavior of the mixture that consists of a base chiral nematic mixture comprising E7 + 3wt% BDH1281 (Merck) doped with 20 wt% of the bimesogenic material 4′,4′-(nonane-1,7-diyl)bis(([1′,1″-biphenyl]-4″-carbo-nitrile), CB9CB [35, 36]. The chiral nematic mixture, which forms a right handed helical structure with a pitch of ≈ 520 nm, was capillary filled into a nominally 5 μm thick device that consisted of glass substrates that were coated with ITO electrodes (to facilitate the application of an electric field along the normal to the device substrates) and anti-parallel rubbed polyimide alignment layers. To ensure that the electric field is orthogonal to the helical axis (a necessary requirement to observe flexoelectro-optic switching) a uniform lying helix (ULH) geometry was required. To form the ULH alignment, the device was heated up to 50ºC in the presence of a 500Hz, 25 V_{pp} square waveform and then cooled down to room temperature in the presence of an applied electric field. All measurements were carried out at a temperature of T = 30 ºC.

The resulting mixture shows enhanced flexoelectro-optic switching when compared to the base E7 + 3wt% BDH1281 mixture, but in contrast to the neat bimesogenic material which exhibits a nematic phase that at substantially elevated temperatures (>100 °C), this mixture can still be operated at room temperature. The electro-optic properties were investigated by applying a 500 Hz square wave voltage waveform using a Tektronix AFG 3022 waveform generator and measuring the switching angle using a combination of a BX51 polarizing

microscope, a Tektronix TBS1154 oscilloscope and high-speed Si photodiode [37]. The results are shown in **FIG. 7(a)**.

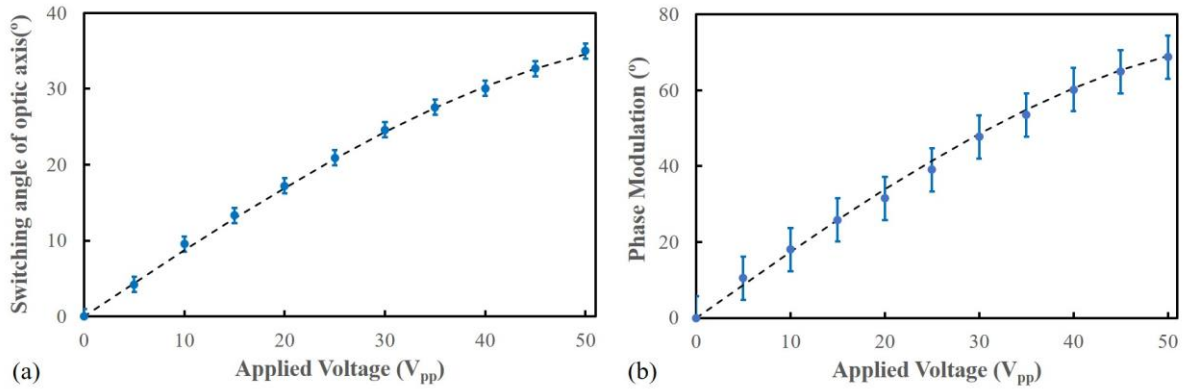

FIG. 7. (a) Flexoelectro-optic switching in the chiral nematic phase of the mixture E7+3wt% BDH1281 + 20wt% CB9CB in a 5µm thick device. The applied voltage was a 500Hz square wave. (a) The flexoelectro-optic switching angle (as measured on a polarizing microscope) is shown as a function of the applied voltage (peak-to-peak) and the dashed line represents a cubic series expansion fit based upon theoretical considerations (see main text). (b) The resulting optical phase modulation in transmission for the same range of flexoelectro-optic switching angles when the device was placed between a pair of quarter-wave plates.

In **FIG. 7(a)** we can see that a peak switching angle of around 35° (±17.5°) was obtained at a switching voltage of $50V_{pp}$. However, at this voltage the helix of the chiral nematic LC begins to unwind and there is some change in the alignment texture; therefore, operation at slightly lower voltages may be preferred. Due to the dielectric anisotropy of the material, and the resulting helix distortion under electric field application, the overall flexoelectro-optic switching behaviour is complex. However, the switching angle can be approximated in terms of a cubic series expansion [38] – this is the dashed line in **FIG. 7a**. This cubic series can be written in terms of the expression for the flexoelectro-optic tilt angle introduced earlier in Section IIIB, plus a correcting cubic term:

$$\chi = \frac{e_1 - e_3}{K_{11} + K_{33}} \frac{E}{q} + \beta \left\{ \frac{e_1 - e_3}{K_{11} + K_{33}} \frac{E}{q} \right\}^3 \qquad (14)$$

where β is treated as a fitting parameter, and is a complex combination of elastic, dielectric and flexoelectric properties [38]. From the dashed line in **FIG. 7a** we can determine the ratio $(e_1 - e_3)/(K_{11} + K_{33})$, which is sometimes referred to as the flexo-elastic ratio for the material, to be 0.924V^{-1} and the value of the fitting parameter β which is β = –1.446; the negative value of β indicates that the dielectric coupling tends to suppress (reduce) the flexoelectro-optic tilt angle.

We then placed this device between quarter-wave plates (**FIG. 4(d) Exp2**) and inserted it into one arm of the Mach-Zehnder interferometer. The device was again driven with a 500Hz square wave (so the switching response to either polarity is taking place in 1 ms), and the interference fringes were recorded on the CCD camera and tracked to extract the resulting optical phase modulation. The resulting phase modulation is shown in **FIG. 7(b)**. We can see that, as expected, the resulting phase modulation is twice the switching angle of the optic axis in the device – this is because the light passes through the device a single time. However, this optical phase modulation is still rather small, with a maximum range of 70° at 50 V_{pp}. There are some losses in this arrangement due to imperfections in the alignment of the helical axis in the flexoelectro-optic device. These alignment imperfections lead to point defects in the LC structure, which in turn results in considerable optical scattering. The demonstration device is therefore somewhat optically inefficient, although it is expected that improvements to the alignment quality would considerably reduce this problem. By choosing the orientation of the device appropriately there is minimal amplitude (or intensity) modulation in this configuration. This is estimated to be less than 10% in amplitude (less than 1dB).

The phase modulation depth can be enhanced if we instead place the device (still between quarter-wave plates) in one arm of the Michelson interferometer. In this case, the light

now passes through the device twice. This is the configuration that we have previously presented using a different mixture that exhibited large switching angles but at very high temperatures (108°C) [23]. The result for the present device is shown in **FIG. 8(a)**. It is immediately noticeable in the figure that the phase modulation has a different curvature from that shown in **FIG. 7** for the switching angle and single-pass phase modulation behaviour, with the curvature being reversed at lower voltages. **FIG. 8(b)**, which presents the result when the light passes through the device four times, shows similar qualitative behaviour to the two-pass case. This effect happens because of the change in retardation of the LC layer under an applied voltage. The material used here has a significant dielectric anisotropy (as noted earlier, for E7 only at room temperature $\Delta\varepsilon$ = 14), and therefore under the application of the electric field there is a tendency for the helix of the chiral nematic LC to distort. In the configuration used here, with the electric field direction and light propagation direction perpendicular to the helical axis, this leads to a reduction in the effective optical anisotropy as the electric field amplitude was increased. To first order this reduction is quadratic in the applied electric field [38].

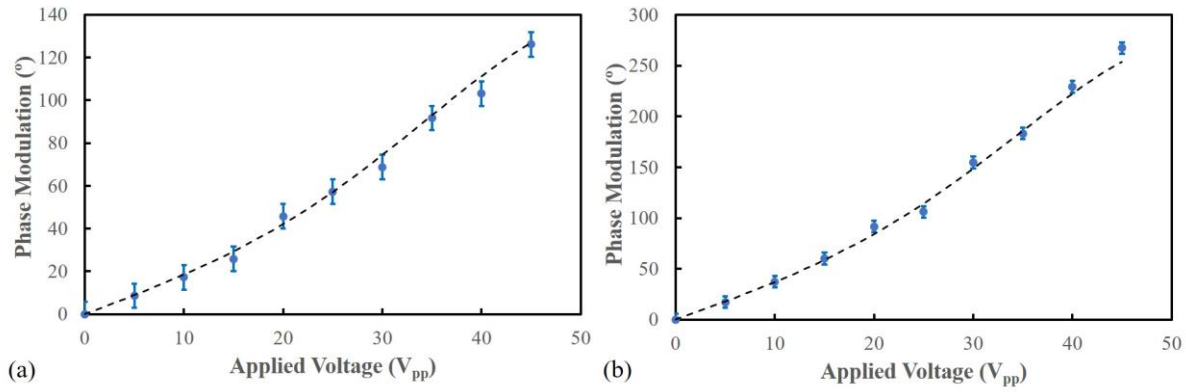

FIG. 8. Phase modulation as a function of the applied voltage (peak-to-peak) for the flexoelectro-optic device consisting of the chiral nematic mixture E7+3wt% BDH1281 + 20wt% CB9CB for multi-pass geometries: (a) two-pass and (b) four-pass configurations. The thickness of the device was nominally 5 µm. The data points represent the results from the experiments and the result from the model(s) are the black dashed lines. The precise form of

the behaviour depends on the orientation of the device, which in this case has been chosen to minimise the amplitude (or intensity) modulation to keep it below 10%.

When the flexoelectro-optic LC device was placed between a pair of quarter-wave plates and the phase shift was measured using polarized light (the configuration for the one-pass transmission measurement results shown in **FIG. 7(b)**) then the phase modulation follows the tilt angle of the optical axis, as can be seen by comparing **FIG. 7(a)** and **FIG. 7(b)**. However, when a mirror is placed behind the second quarter-wave plate the behaviour changes. The configuration experienced by the light path is now: quarter-wave plate, LC device (first pass), quarter-wave plate, mirror, quarter-wave plate, LC device (second pass), quarter-wave plate. Now, changes in the effective birefringence of the LC layer under the application of an electric field distorts the optical phase change as a function of tilt angle behaviour, making it non-linear, and resulting in the curves seen in **FIG. 8**. The shape of these curves would be qualitatively similar to those shown in **FIG. 7** if a polarizer were placed between the second quarter-wave plate and the mirror.

In **FIG. 7(a)** the switching angle of the flexoelectro-optic LC device for a voltage of $45V_{pp}$ at 500Hz is over a range of 32.5° (i.e. ±16.25°). The resulting optical phase change available in a one-pass configuration is then twice this value, being 65° for $45V_{pp}$ as shown in **FIG. 7(b)**. Although the shapes of the curves are different, we can see that in the two-pass case the maximum optical phase modulation is again doubled (to a range of 130° for $45V_{pp}$ in **FIG. 8(a)**. In the four-pass case it is further doubled to a maximum range of 260° for $45V_{pp}$, as seen in **FIG. 8(b)**. At this point the optical phase modulation is eight times the flexoelectro-optic switching angle range, which means that full 0 to 2π optical phase modulation would be

available in this arrangement using a flexoelectro-optic device with a switching angle of 45° (±22.5°).

V. CONCLUSIONS

In summary, we have demonstrated two different configurations that allow substantial optical phase modulation on a millisecond timescale at room temperature. Using a pi-cell driven at high voltages in a multi-pass optical arrangement has allowed a boundary layer high-speed switching effect to be exploited, giving full 0 to 2π optical phase modulation in 1 ms. It should be noted that this device used the well-characterized nematic LC, E7, and therefore substantially faster switching times could be obtained by using an optimized mixture (e.g. one with lower rotational viscosity, higher optical birefringence, larger elastic constants). This would therefore pave the way to full 0 to 2π optical phase modulation in sub-millisecond time scales.

Using the flexoelectro-optic effect in chiral nematic LC devices, we have shown enhanced multi-pass optical phase modulation. Modulation of 260° was achieved on a 1 ms time-scale using a material which showed a switching angle of just over 32° at $45V_{pp}$. Full 0 to 2π optical phase modulation could be achieved either using a slightly more optimized mixture (to give a switching angle of ±22.5°) or by using a six-pass optical arrangement. For example, a material developed by Varanytsia and Chien based on the nematic host MLC-2048 (Merck) doped with the bimesogenic compound, CB7CB showed room-temperature switching angles of up to ±40° [22], although this was at somewhat higher applied electric field amplitudes.

A key application of the ideas proposed here is in the development of spatial light modulator technology with sub-millisecond switching over a full phase range. In order to

implement the multi-pass configurations using such technology it would be necessary to ensure that each modulating pixel is re-imaged onto the same modulating pixel in subsequent passes. For two-pass operation this can be achieved by integrating a mirror into the back-plane of the device. For four-pass (and higher) arrangements there are two possible approaches. For example, Peng et al. have demonstrated a very interesting integrated multi-pass configuration when optimising the phase modulation available using blue-phase LC technology [39]. This solution is very elegant, but the integrated mirrors do substantially reduce the useable mark-space ratio of the pixels in a device. An alternative approach to this would necessitate an imaging system, such as a folded four-*f* system. In this arrangement light is incident on an SLM with an integrated mirror back-plane. The reflected light is then passed through a lens, which is placed its focal length from the spatial light modulator, and on to a mirror, which is placed at the focal length of the lens behind the lens. The light is hence reflected and precisely imaged back through the lens onto the same pixel in the SLM through which it first passed. The light therefore passes four times through each individual pixel. Further higher-pass configurations can be envisaged, although the imaging arrangements would not be convenient to implement.

A further concern for the practical technological implementation of the ideas presented here are the drive voltages used. These are up to $50V_{pp}$ ($\pm 25V$), which are somewhat higher than normally used in spatial light modulators with integrated Silicon back-planes. However, it is anticipated that these drive voltages could be reduced through material choice and/or optimization. In the pi-cell demonstration presented here, the work was undertaken with the standard nematic material, E7. Choosing (or potentially developing) a material with higher dielectric anisotropy and high optical birefringence would allow the drive voltages to be substantially reduced. The flexoelectro-optic phase modulator was constructed using an in-house developed mixture. Again, optimisation of the material to enhance its flexoelectric

coefficient and increase its birefringence would allow the use of thinner layers at reduced voltages.

In future work, we aim to develop the concepts introduced here to demonstrate multi-pixel phase modulators. These have exciting applications in areas such as optical beam steering, programmable diffractive elements, and micromanipulation.

Acknowledgements

This research was supported by the Engineering and Physical Sciences Research Council (UK) (grant numbers EP/M017923/1 and, EP/M015726/1), and the European Space Agency contract 4000125232/18/NL/AR/zk.

References

[1] S. Mias and H. Camon, A review of active optical devices: II. Phase modulation, J. Micromech. Microeng. **18**, 083002 (2008).

[2] D. G. Grier, A revolution in optical manipulation, Nature **424**, 810 (2003).

[3] C. Maurer, A. Jesacher, S. Bernet, and M. Ritsch-Marte, What spatial light modulators can do for optical microscopy, Laser Photonics Rev. **5**, 81 (2011).

[4] R. Lynge Eriksen, V. Ricardo Daria, J. Glückstad, R. Eriksen, V. Daria, and J. Gluckstad, Fully dynamic multiple-beam optical tweezers, Opt. Express **10**, 597 (2002).

[5] D. J. McKnight, K. M. Johnson, and R. A. Serati, 256 × 256 liquid-crystal-on-silicon spatial light modulator, Appl. Opt. **33**, 2775 (1994).

[6] J. A. Davis, D. E. McNamara, D. M. Cottrell, and T. Sonehara, Two-dimensional polarization encoding with a phase-only liquid-crystal spatial light modulator, Appl. Opt. **39**, 1549 (2000).

[7] N. Chattrapiban, E. A. Rogers, D. Cofield, W. T. Hill III, and R. Roy, Generation of nondiffracting Bessel beams by use of a spatial light modulator, Opt. Lett. **28**, 2183 (2003).

[8] S. E. Broomfield, M. A. A. Neil, E. G. S. Paige and G. G. Yang, Programmable binary phase-only optical device based on ferroelectric liquid crystal SLM, Electronics Letters **28**, 26 (1992).

[9] L. Vicari, Optical Applications of Liquid Crystals, CRC Press, 41-57 (2016).

[10] S. P. Kotova, A. M. Mayorova, E. P. Pozhidaev and S. A. Samagin, Simulation of spatial phase light modulators based on the ferroelectric liquid-crystals, J. Phys.: Conf. Ser. **1096**, 012017 (2018).

[11] Z. Feng and K. Ishikawa, Phase modulator mode based on the pre-transitional effect of antiferroelectric liquid crystals, Opt. Lett. **43**, 251 (2018).

[12] U. Efron, S. T. Wu, and T. D. Bates, Nematic liquid crystals for spatial light modulators: recent studies, J. Opt. Soc. Am. B **3**, 247 (1986).

[13] J. Albero, P. García-Martínez, J. Luis Martínez, and I. Moreno, Second order diffractive optical elements in a spatial light modulator with large phase dynamic range, Optics and Lasers in Engineering, **51**, 111 (2013).

[14] Y. Huang, Z. He, and S.-T. Wu, Fast-response liquid crystal phase modulators for augmented reality displays, Opt. Express **25**, 32757 (2017).

[15] E. Hallstig, J. Stigwall, M. Lindgren and L. Sjoqvist, Laser beam steering and tracking using a liquid crystal spatial light modulator, Proc. SPIE **5087,** 13 (2003).

[16] A. Jesacher and M. Booth, Parallel direct laser writing in three dimensions with spatially dependent aberration correction, Opt. Express **18**, 21090 (2010).

[17] Y. Lee, D. Franklin, F. Gou, G. Liu, F. Peng, D. Chanda, and S.-T. Wu, Two-photon polymerization enabled multi-layer liquid crystal phase modulator, Sci Rep **7**, 16260 (2017).

[18] Z. He, G. Tan, D. Chanda, and S.-T. Wu, Novel liquid crystal photonic devices enabled by two-photon polymerization, Opt. Express **27**, 11472 (2019).

[19] Z. He, Y.-H. Lee, F. Gou, D. Franklin, D. Chanda, and S.-T. Wu, Polarization-independent phase modulators enabled by two-photon polymerization, Opt. Express **25**, 33688 (2017).

[20] Z. He, F. Gou, R. Chen, K. Yin, T. Zhan, and S. -T. Wu, Liquid Crystal Beam Steering Devices: Principles, Recent Advances, and Future Developments, Crystals **9**, 292 (2019).

[21] J. S. Patel and R. B. Meyer, Flexoelectric electro-optics of a cholesteric liquid crystal, Phys. Rev. Lett. **58**, 1538 (1987).

[22] A. Varanytsia and L. C. Chien, Giant Flexoelectro-optic Effect with Liquid Crystal Dimer CB7CB, Sci. Rep. **7**, 41333 (2017).

[23] J. A. J. Fells, X. Wang, S. J. Elston, C. Welch, G. H. Mehl, M. J. Booth, and S. M. Morris, Flexoelectro-optic liquid crystal analog phase-only modulator with a 2π range and 1 kHz switching, Opt. Lett. **43**, 4362 (2018).

[24] S.-T. Wu and C.-S. Wu, High-speed liquid-crystal modulators using transient nematic effect, J. Appl. Phys. **65**, 527(1989).

[25] R. Chen, Y. Huang, J. Li, M. Hu, J. Li, X. Chen, P. Chen, S.-T. Wu and Z. An, High-frame-rate liquid crystal phase modulator for augmented reality displays, Liquid Crystals, **46**, 309 (2019).

[26] G. D. Love, A. K. Kirby, and R. A. Ramsey, Sub-millisecond, high stroke phase modulation using polymer network liquid crystals, Opt. Express **18**, 7384 (2010).

[27] P. J. Bos and K. Rickey Koehler/beran, The pi-Cell: A Fast Liquid-Crystal Optical-Switching Device, Molecular Crystals and Liquid Crystals **113**, 329 (1984).

[28] W. Ye, Z. Li, R. Yuan, P. Zhang, T. Sun, M. Cai, X. Wang, J. Zhu, Y. Sun, and H. Xing, Accurate measurement of the twist elastic constant of liquid crystal by using capacitance method, Liquid Crystals **46**, 349 (2019).

[29] P. C.-P. Chao, Y.-Y. Kao, and C.-J. Hsu, A new negative liquid crystal lens with multiple ring electrodes in unequal widths, IEEE photonics journal, **4** (1), 250 (2012).

[30] B. I. Outram and S. J. Elston, Frequency-dependent dielectric contribution of flexoelectricity allowing control of state switching in helicoidal liquid crystals, Phys. Rev. E **88**, 012506 (2013).

[31] P. Yeh and C. Gu, Optics of Liquid Crystal Displays. *John Wiley & Sons, Inc., Publication.* Chap 4 173-277 (2010).

[32] C. S. Caldwell, J. R. Hall, and A. L. Babb, Mach-Zehnder Interferometer for Diffusion Measurements in Volatile Liquid Systems, Review of Scientific Instruments **28**, 816 (1957).

[33] H. G. Walton and M. J. Towler, On the response speed of pi-cells, Liquid Crystals **27**, 1329 (2000).

[34] C. Sun, Multiplexing of fiber-optic acoustic sensors in a Michelson interferometer configuration, Opt. Lett. **28**, 1001 (2003).

[35] C. Bacchiocchi, M.-G. Tamba, G. H. Mehl, A. Arcioni, I. Miglioli and C. Zannoni, EPR study of the polydomain structure of the twist-bend nematic phase of CB9CB in the bulk, Liquid Crystals, **45**, 2109 (2018).

[36] V. P. Panov, R. Balachandran, M. Nagaraj, J. K. Vij, M. G. Tamba, A. Kohlmeier, and G. H. Mehl, Microsecond linear optical response in the unusual nematic phase of achiral bimesogens, Appl. Phys. Lett. **99**, 261903 (2011).

[37] F. Castles, S.C. Green, D.J. Gardiner, S.M. Morris, and H.J. Coles, Flexoelectric coefficient measurements in the nematic liquid crystal phase of 5CB, AIP Advances **2** (2), 022137 (2012).

[38] D. R. Corbett and S. J. Elston, Modeling the helical flexoelectro-optic effect, Physical Review E **84**, 041706 (2011).

[39] F. Peng, Y.-H. Lee, Z. Luo, and S.-T. Wu, Low voltage blue phase liquid crystal for spatial light modulators, Opt. Lett. **40**, 5097 (2015).